CERES results on low-mass electron pair production in Pb–Au collisions

I. Ravinovich for the CERES Collaboration:

G. Agakichiev[a], R. Baur[b], P. Braun-Munzinger[c], F. Ceretto[d], A. Drees[b], S. Esumi[b], U. Faschingbauer[b,d], Z. Fraenkel[e], Ch. Fuchs[d], E. Gatti[f], P. Glässel[b], C.P. de los Heros[e], P. Holl[g], Ch. Jung[b], B. Lenkeit[b], M. Messer[b], Y. Panebrattsev[a], A. Pfeiffer[b], J. Rak[d], I. Ravinovich[e], S. Razin[a], P. Rehak[g], M. Richter[b], M. Sampietro[f], N. Saveljic[a], J. Schukraft[h], S. Shimanskiy[a], W. Seipp[b], E. Socol[e], H.J. Specht[b], J. Stachel[b], G. Tel-Zur[e], I. Tserruya[e], T. Ullrich[b], C. Voigt[b], C. Weber[b], J.P. Wessels[b], T. Wienold[b], J.P. Wurm[d], V. Yurevich[a]

[a] JINR, Dubna, Russia
[b] Universität Heidelberg, Germany
[c] GSI, Darmstadt, Germany
[d] Max-Planck-Institut für Kernphysik, Heidelberg, Germany
[e] Weizmann Institute of Science, Rehovot, Israel
[f] Politecnico di Milano, Italy
[g] Brookhaven National Laboratory, Upton, USA
[h] CERN, Geneva, Switzerland

The CERES/NA45 collaboration measured, at the CERN SPS, low-mass electron pair production in Pb–Au collisions at 158 A GeV/c incident momentum. In this paper we present an analysis of the data taken during the SPS Pb-beam period in the fall of 1995. The results confirm previous findings of CERES showing that the pair production in the mass range $0.2 < m_{ee} < 1.5$ GeV/c^2, when scaled to the ion case with the event multiplicity, is enhanced over the expected yield from the known hadronic sources in pp collisions. A comparison of the results for different multiplicity bins indicates that the excess increases faster than linearly with charged-particle multiplicity. We also present the transverse-momentum distributions of the observed pairs.

1. INTRODUCTION

CERES is an experiment dedicated to the measurement of low-mass electron-positron pairs and direct photons produced in ultra-relativistic heavy-ion collisions at the CERN SPS. These observables are important probes for studying the dynamics of the collision and in particular, the early stages where formation of the quark-gluon plasma (QGP) and restoration of chiral symmetry are expected to take place. A crucial feature of dileptons is their ability to reflect the initial temperature of the system and the nature of the matter formed, the conjectured QGP, through quark annihilation ($q\overline{q} \rightarrow l^+l^-$) or a high-density hadron gas through pion annihilation ($\pi^+\pi^- \rightarrow l^+l^-$). Furthermore, dileptons offer the opportunity to measure the vector mesons through their leptonic decays. This is of particular importance with regard to the ρ meson. Due to its very short lifetime

compared to the typical fireball lifetime, most of the ρ mesons produced in the collision will decay inside the interaction region. If the temperature and/or the baryon density are high enough for partial chiral symmetry restoration to take place, the ρ mesons will decay with a reduced mass leading to a detectable signal in the low-mass dilepton spectrum.

The interest in the measurement of low-mass dileptons is matched by the difficulty of their experimental detection. The main experimental problem is the huge *combinatorial background* of uncorrelated lepton pairs originating from random combinations of tracks from unrecognized π^0 Dalitz decays and gamma conversions in the same event. This background strongly increases as the coverage moves to the low-mass and low-p_t regions and it has a quadratic dependence on the charged-particle multiplicity.

In order to perform this interesting and challenging experiment CERES has developed a dedicated spectrometer which is briefly described in the next section. With this spectrometer, CERES has carried out over the last five years a systematic research programme with p, S and Pb beams. A short review of CERES results with the proton and S beams is given in Section 3. In this presentation, we concentrate on the final analysis of the Pb-Au data taken in the fall of 1995. The data analysis procedure is described in detail in Section 4. The results are presented in Section 5 and a summary and outlook are given in Section 6.

2. EXPERIMENTAL SETUP

The CERES spectrometer (Fig. 1) is optimized to measure low-mass electron pairs from about 50 MeV/c^2 up to beyond 2 GeV/c^2, limited at the upper end by statistics. It covers the pseudorapidity region $2.1 < \eta < 2.65$ with 2π azimuthal symmetry and accepts a very broad range of p_t. A detailed description of the original CERES set-up can be found in [1]. Here we describe the most relevant features of the detector. Electron identification and directional tracking are based on two azimuthally symmetric Ring Imaging Cherenkov (RICH) counters, one (RICH-1) situated before, the other (RICH-2) after a superconducting double solenoid. The set-up includes also external tracking detectors: a doublet of silicon radial-drift detectors located downstream of the target and before RICH-1, and a multiwire proportional chamber with pad readout downstream of RICH-2. There are five essential features in the design of the CERES spectrometer of particular importance for the detection of electron pairs and for its operation at high multiplicities: (i) The spectrometer is almost "blind" to hadrons. The radiators of the RICH detectors are filled with CH_4 at atmospheric pressure, which has a threshold of $\gamma_{th} \simeq 32$. This high value ensures that essentially only electrons emit Cherenkov radiation when traversing the detector. (ii) The UV detectors are placed upstream of the target, and thus they are not traversed by the intense flux of forward-going charged particles produced in the interaction. (iii) The amount of material within the acceptance (not counting the target) is kept below 1% of a radiation length. This minimizes the amount of gamma conversions which would otherwise contribute to the combinatorial background. (iv) The shape of the magnetic field results in a field-free region in RICH-1. This is of extreme importance since it allows to recognize and reject π^0 Dalitz decays and conversion pairs by their small opening angle. (v) The external tracking detectors are essential to cope with the high multiplicity environment in central Pb–Au collisions. They add redundancy to the directional tracking of the RICH detectors and reduce the amount of fake tracks to a

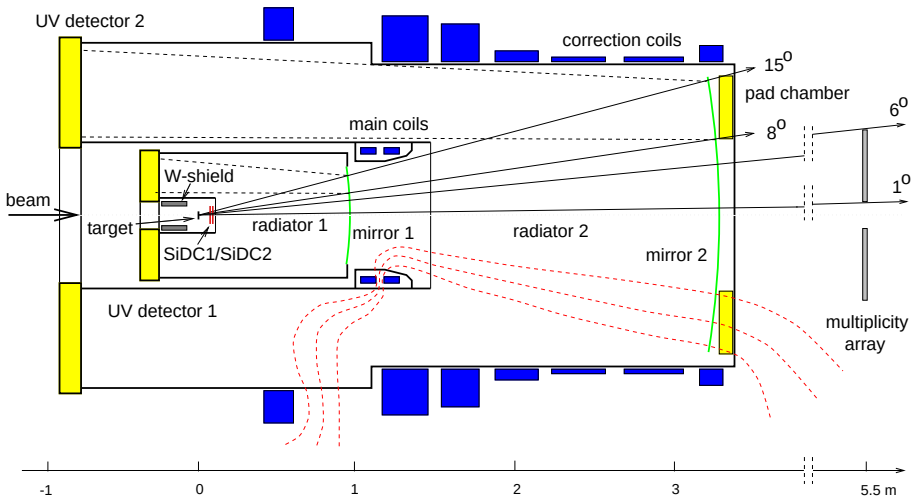

Figure 1. Schematic view of the CERES spectrometer used in the 1995 run.

negligible level. Furthermore, they provide additional background rejection and improve the momentum and mass resolutions of the spectrometer.

3. REVIEW OF PREVIOUS CERES RESULTS

CERES has completed a systematic physics programme including the measurements of electron pairs in p–Be (a very good approximation to p-p collisions) and p–Au collisions at 450 GeV/c [2,3], S–Au collisions at 200 A GeV [4] and Pb–Au collisions at 158 A GeV [5]. This systematic approach has established a very interesting result: the observation of a strong enhancement of low-mass electron pairs in S–Au collisions [4], indicating the onset of a new source, beyond the mere superposition of p–p collisions, whereas no enhancement was observed in p–Be and p–Au collisions. This enhancement is confirmed by the results obtained with the Pb beam [5] which will be discussed in this paper.

The S results are shown in Fig. 2 (left). The data are normalized to represent the pair density per charged-particle density within the CERES rapidity acceptance. This is a convenient way to normalize the data. It assumes that the particle production ratios remain unchanged in the different systems and therefore allows us to scale the dilepton yield from proton-proton to nucleus-nucleus collisions with the event multiplicity. Statistical (vertical bars) and systematic (brackets) errors are plotted independent of each other. In the absence of new physics, electron pairs are expected to originate from the known hadronic sources: Dalitz decays, π^0, η, $\eta' \rightarrow e^+e^- \gamma$, $\omega \rightarrow e^+e^- \pi^o$, and resonance decays, ρ_0, ω and $\phi \rightarrow e^+e^-$. The invariant-mass spectrum resulting from all these sources was calculated with a generator [4]. The relative meson abundances were taken from p–Be [6] and they were assumed to be proportional to $\langle dN_{ch}/dy \rangle$. For details on the generator see [4].

The full line (with shaded region) in Fig. 2 represents the summed contribution of all these sources, as measured in p-p collisions. The measured spectrum has a different shape and shows a strong enhancement over the hadronic contributions at masses m $>$ 0.2 GeV/c^2, reaching one order of magnitude around m $\sim$ 0.4 GeV/c^2. As a quantitative measure of the observed excess we define the enhancement factor as the integral of the

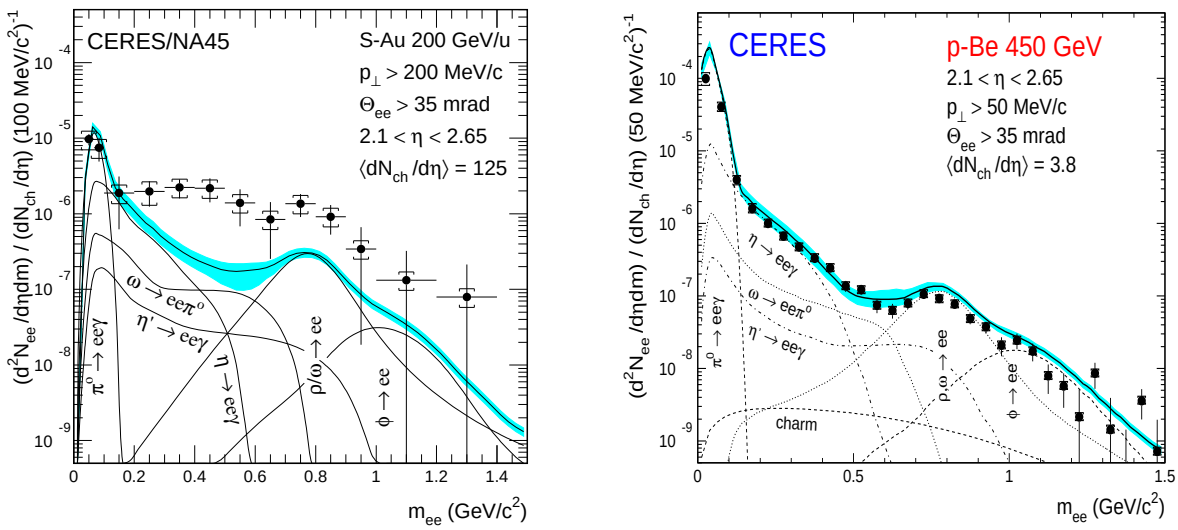

Figure 2. Mass spectra of inclusive e^+e^--pairs in S–Au (left) [4] and p–Be (right) [3] collisions showing the data (full circles) and the various contributions from hadron decays. Systematic (brackets) and statistical errors (bars) are plotted independently of each other. The shaded regions indicate the systematic error on the summed contributions.

data over the integral of the predicted sources in the invariant mass range $0.2 < m_{ee} < 1.5$ GeV/c^2, which results in $5.0 \pm 0.7(\text{stat.}) \pm 2.0(\text{syst.})$. An enhancement of low-mass muon pairs has also been observed by HELIOS-3 [7] in S-W collisions and by NA38 in S-U collisions [8], both at 200 A GeV.

As a basis for comparison with nuclear collisions, CERES collected a large sample of electron pairs from 450 GeV p–Be and p–Au collisions in 1993 [2,3]. The analysis of the invariant mass spectrum measured in p-Be shows very good agreement with the predictions based on the known hadron decay sources (Fig. 2 (right)), and there is no need to invoke any unconventional source (within the present systematic errors). The same conclusion holds in the case of p–Au collisions.

The S result has triggered considerable theoretical activity. For recent reviews see [9,10]. It was clear that the explanation of the enhancement will require an additional source not present in the pp case. A possible explanation was immediately proposed based on the properties of the observed dilepton excess: its onset at $m_{ee} \sim 2m_\pi$, the persistence of the enhancement in the ρ mass region and the possibility of a quadratic dependence with multiplicity suggest that it is dominated by two-pion annihilation $\pi^+\pi^- \rightarrow l^+l^-$ [4,11] providing first evidence of thermal radiation emitted by the high density hadronic matter formed in these collisions. Numerous calculations have been reported, which have all included the pion annihilation channel [12–16]. An interesting observation is that all these calculations agree with each other within a factor of two in spite of the very different assumptions used to describe the space-time evolution of the collision. But most significantly, all these approaches account for a sizeable fraction of the observed excess, but they all fail to reproduce the data in the mass region $0.2 < m_{ee} < 0.5$ GeV/c^2.

In order to fully account for the excess in this mass region, the models invoke in addition in-medium modifications of the vector mesons. In particular, Li, Ko and Brown [12] were

the first to propose a decrease of the ρ-meson mass inside the dense and hot medium as a precursor of chiral symmetry restoration [17–19]. With this approach excellent agreement has been achieved with the CERES and HELIOS-3 data [12,13]. Recently, calculations [14,15] have been performed using a ρ-meson spectral function which includes the pion modification in the nuclear medium and ρ scattering with baryons and mesons. This leads to a strong broadening of the ρ-meson resonance, thereby helping to enhance the yield of low-mass dileptons. These calculations reproduce the CERES and HELIOS-3 results equally well as the dropping ρ-mass scenario. For a broader review see other talks at this conference [20,21].

4. DATA ANALYSIS

The results presented here were obtained from the analysis of the data taken in 9 days during the SPS Pb beam period in the fall of 1995. The data were collected with an interaction trigger corresponding to a charged-particle density $dN_{ch}/d\eta \geq 100$, i.e. to the top 35% of the geometrical cross section with an average multiplicity of $\langle dN_{ch}/dy \rangle = 220$ in $\eta = 2$–3. This trigger was derived from an array of scintillator counters located downstream of the spectrometer. A total of 9 million events were analyzed.

4.1. Track reconstruction

In the present analysis, we take full advantage of the external tracking detectors for the track reconstruction. The momentum is determined by combining all measurements along the track, three space points and two angles, each weighted by the detector resolution including multiple scattering. As a result the relative momentum resolution at high momenta is better by nearly 50% compared to the S data analysis which was based only on the two RICH detectors.

The track reconstruction scheme includes several important steps: first the event vertex is reconstructed using the doublet of silicon drift detectors. Next, each track is extrapolated from the vertex into RICH-1 to match independently reconstructed ring candidates. All track segments are further extrapolated through the magnetic field into the pad chamber. Since we do not know the momentum and the deflection in the magnetic field, every hit in the pad chamber within a certain window is used for the track reconstruction, but only the small fraction which matches a Cherenkov ring in RICH-2 is accepted. The size of this window is determined in the azimuthal direction by a cut on transverse momentum $p_t \geq 50$ MeV/c and in the polar angle by $\pm 3\sigma$, where σ is the total resolution of the two RICH detectors which amounted to $\sim$1.8 mrad. Finally, cuts on the quality of the Cherenkov rings in both RICHes as well as on the track match in radial direction between individual detectors reduce the amount of fake tracks to the percent level.

The track reconstruction efficiency is determined with a Monte-Carlo simulation. Individual electron-positron pairs from meson decays are generated using the event generator described in the previous section. The full detector response is modeled with a GEANT-based [22] simulation and the specific detector properties. The simulated pairs are overlayed on real events and then analyzed with the same software package as used in the real data analysis. On average about 50% of the tracks are reconstructed. No significant dependence of the track reconstruction efficiency on transverse momentum p_t, polar angle θ of the tracks and the pair opening angle θ_{ee} is observed.

4.2. Pair reconstruction

The overwhelming majority of the reconstructed tracks originate from π^0 Dalitz decays and gamma conversions. Combining all tracks of a given event into pairs leads to a huge combinatorial background and, as mentioned in the introduction, this is the major difficulty of the experiment. In order to reduce this combinatorial background we exploit the kinematical characteristics of such decays. First we make use of the fact that electrons from conversions and π^0 Dalitz decays have soft p_t spectra, compared to electrons from heavier meson decays, and therefore only tracks with $p_t > 200$ MeV/c are used in the final pairing. This is the most powerful rejection cut of the whole analysis chain but is by far not sufficient.

The next step is to identify *fully reconstructed* pairs from gamma and π^0 Dalitz decays. Here we exploit another kinematical characteristic of such decays, namely the small pair opening angle. The small opening angle gives rise to two unresolved rings in RICH-1 (mostly from conversions) opened by the magnetic field, producing a typical V pattern, or to two intersecting rings in RICH-1 (mostly from π^0 Dalitz decays). Thus, tracks belonging to pairs with an opening angle of $\theta < 35$ mrad are not used for further pairing. If the two tracks have a $p_t > 200$ MeV/c they are kept in the sample and marked as assigned tracks. If one track has a $p_t > 200$ MeV/c whereas the other one has $100 < p_t < 200$ MeV/c, both tracks are removed from the sample.

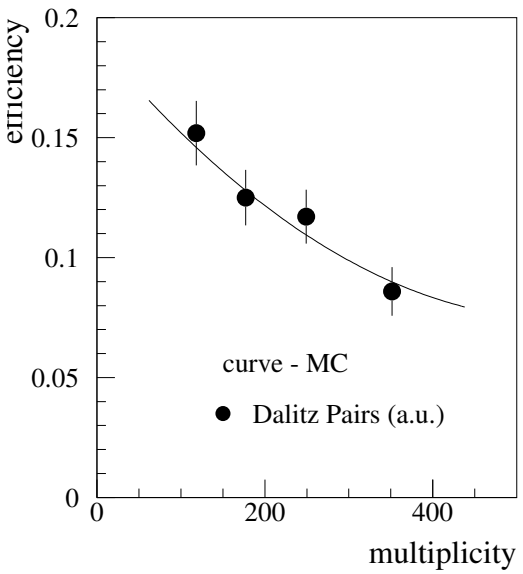

Figure 3: Pair reconstruction efficiency as a function of multiplicity. The curve represents the Monte-Carlo study of the efficiency whereas the points represent the efficiency derived from a sample of reconstructed π^0 Dalitz decays.

At this stage of the analysis we still have a large contamination from gamma conversions and π^0 Dalitz decays where only one track has been reconstructed and the other one was lost mainly due to the p_t-cut and finite reconstruction efficiency. The problem now is to recognize and reject these *partially reconstructed* conversions and Dalitz decays. Here we exploit the fact that the space up to and including RICH-1 is field-free and consequently the missing tracks have a very high probability to be detected in the silicon detectors and in RICH-1, thereby providing an excellent opportunity to recognize them. Most of the conversions can be identified by a double dE/dx signal in each of the two silicon detectors. Single tracks which are matched to such a pattern in the silicon detectors are rejected as members of an unrecognized conversion. Single tracks are also rejected as members of an unrecognized conversion if the ring in RICH-1 has a large number of Cherenkov photon hits and if it is matched to two close hits (within the double-ring resolution of RICH-1) in each of the silicon detectors. Finally, if the missing track is (partially) detected in the silicon detectors and in RICH-1, the pair opening angle becomes accessible and this offers an indispensable tool to reject

tracks from partially reconstructed π^0 Dalitz decays. On these grounds, tracks with a close ring in RICH-1 having a corresponding trajectory in the silicon detectors system are rejected as a member of an unrecognized Dalitz decay.

All tracks with $p_t > 200$ MeV/c surviving the rejection cuts are then combined into pairs, giving rise to an unlike (e^+e^-) pair sample and a like-sign (e^+e^+ and e^-e^-) pair sample.

The rejection cuts described above reduce considerably the combinatorial background and, although they also reduce of the number of reconstructed pairs, the overall improvement of the signal to background (S/B) ratio is more than one order of magnitude. The pair reconstruction efficiency resulting from the successive rejection steps was studied with the Monte-Carlo method described previously. The efficiency was also determined using fully reconstructed π^0 Dalitz pairs for which a large sample with a good signal to background ratio can be easily obtained. Both methods are in very good agreement with each other. The final pair reconstruction efficiency as obtained from the Monte-Carlo is about 12%. The reconstruction efficiency was also studied as a function of the event multiplicity. The results using the Monte-Carlo method (curve), and the sample of π^0 Dalitz pairs (full circles), are shown in Fig. 3. One sees a significant effect, the reconstruction efficiency decreases from 16% at low $dN_{ch}/d\eta$ to 7% at high $dN_{ch}/d\eta$. No significant mass dependence of the efficiency is observed.

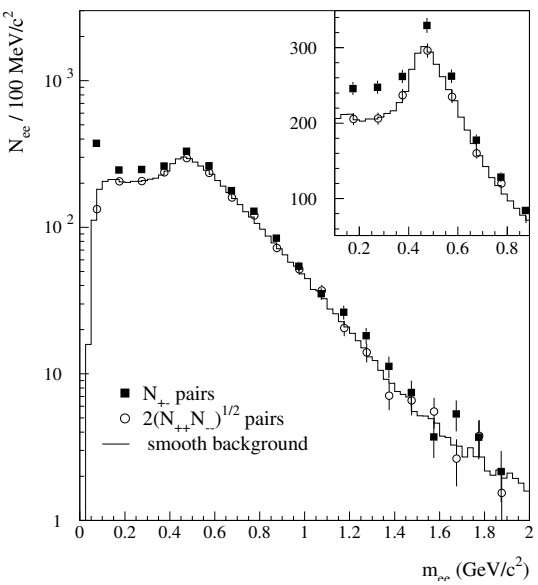

Figure 4: Comparison of the mass spectra of unlike- and like-sign pairs before efficiency correction. The histogram gives the smoothed like-sign spectrum (see text). The insert displays the low-mass region on a linear scale.

4.3. Signal determination

The combinatorial background in the e^+e^- sample is assumed to be equal to the total yield of like-sign pairs, defined as twice the geometrical mean of the numbers $N_{e^+e^+}$ and $N_{e^-e^-}$, i.e. $B = 2\ (N_{e^+e^+}\ N_{e^-e^-})^{1/2}$. The pair signal S is then obtained by subtracting the like-sign contribution from the unlike-sign pairs as $S = N_{e^+e^-} - B$. The invariant-mass distributions of the unlike-sign pairs and of the background B are shown in Fig. 4. In order to reduce statistical bin-to-bin fluctuations, a smooth like-sign spectrum was created from a large sample of tracks which are generated randomly according to the measured p_t, θ and ϕ distributions of tracks from like-sign pairs. By this technique, an excellent description of the like-sign mass, p_t and opening angle distributions is achieved in all observed phase space selections. The final sample contains 1038 ± 55 reconstructed e^+e^- pairs for invariant masses below 0.2 GeV/c^2 at a signal-to-background ratio of 1.05. For masses above 0.2 GeV/c^2 we find 5834 e^+e^-, 2494 e^+e^+, and 2696 e^-e^- pairs resulting in

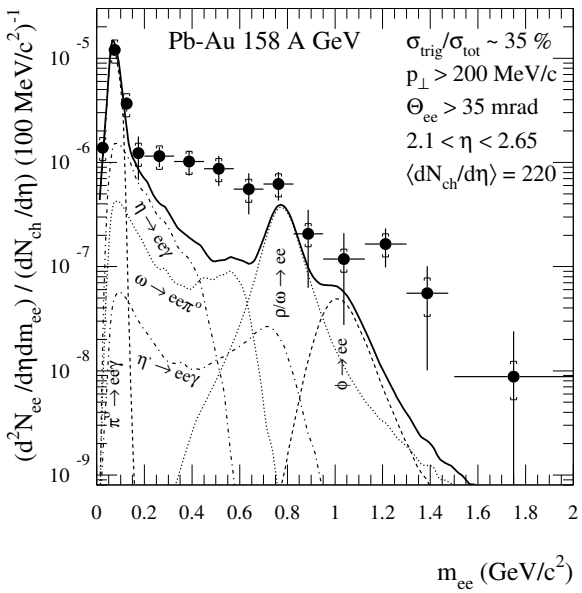

Figure 5. Inclusive e^+e^- mass spectrum in 158 A GeV Pb–Au collisions normalized to the observed charged-particle density. See caption of Fig. 2 for more details.

a net signal of 648 ± 105 pairs with a signal-to-background ratio of 1/8.

A noticeable feature of Fig. 4 is the similar spectral shape (within the present statistics) of the signal and the combinatorial background for masses m > 200 MeV/c^2, raising the question whether the combinatorial background has been subtracted correctly. However, as will be shown later, the mass spectrum of the signal changes significantly with the event multiplicity whereas the shape of the combinatorial background remains, as expected, unchanged.

Another serious concern is that in view of the poor S/B ratio for masses m > 200 MeV/c^2, there is a danger of creating a signal out of statistical fluctuations when optimizing the cuts along the analysis chain. We have made several checks to validate the correctness of the analysis and the stability of the final results. The value of each rejection cut was adjusted by optimizing the quantity ϵ^2/B (which is a measure of the magnitude of the signal in a background-free situation) where the pair reconstruction efficiency ϵ is obtained from the Monte-Carlo simulation while the background B is the measured like-sign pair background; this procedure disregards the size of the signal itself. In an independent analysis the signal and the S/B ratio were studied as a function of each cut value. Their systematic behavior was used to derive the value of each cut. Both methods yielded very similar values for all the rejection cuts with differences typically of the order of 10% or less. The resulting variations in the final signal are of the order of 20% and these are taken as an indication of the systematic errors induced by the analysis. To check the stability of the results all background rejection cuts were varied simultaneously and at random within a window of $\pm$ 15% around the optimal values. After efficiency correction the result remained within the systematic errors. In a second check, the analysis was repeated (i) without the final combinatorial background rejection cuts and (ii) with much relaxed cuts in the tracking but with the final rejection cuts. The S/B ratio deteriorated from 1/8 to 1/25 and 1/30 respectively, but the absolute signal after the corresponding

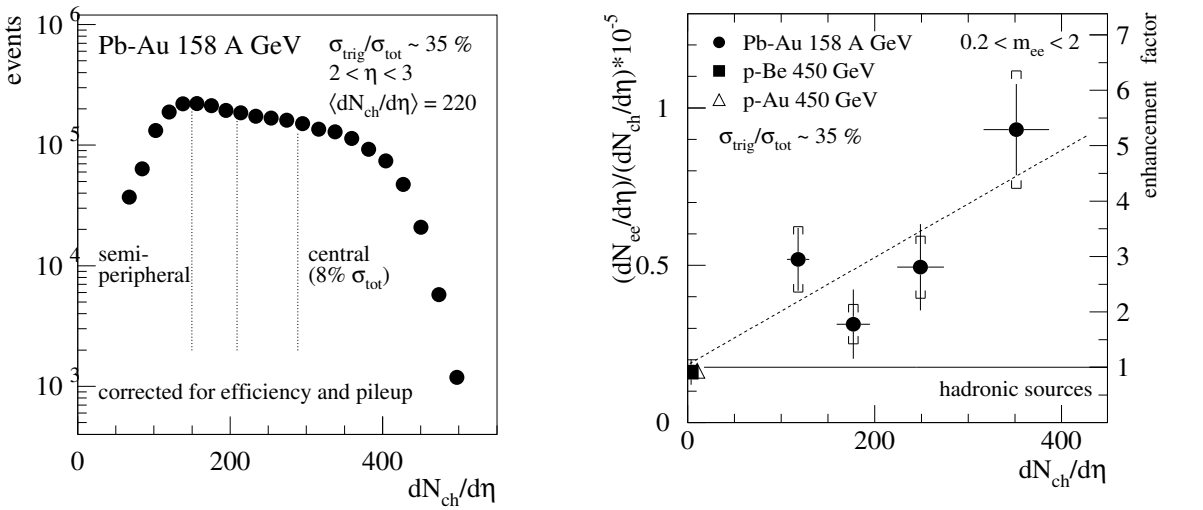

Figure 6. Multiplicity distribution $dN_{ch}/d\eta$ for $2 < \eta < 3$ as measured by the target telescope, corrected for efficiency and pile-up (left) and pair density per charged particle density as a function of charged particle density for $0.2 < m_{ee} < 2$ GeV/c^2 (right).

efficiency correction remained again stable within errors.

5. RESULTS

5.1. Invariant mass spectrum

The resulting invariant mass spectrum of e^+e^- pairs is shown in Fig. 5 together with the expected contributions from hadron decays [5]. It is normalized to represent pair density per charged-particle density with an average $\langle dN_{ch}/d\eta \rangle = 220$ in $\eta = 2$–3. The data are corrected for the pair reconstruction efficiency. The statistical errors of the data are shown as bars whereas systematic errors are given separately as brackets. The latter contain contributions from the uncertainties in the calculation of the charged-particle densities, the pair reconstruction efficiency, the absolute background level and the background smoothing procedure. They add up to 25-40%, depending on mass, and are strongly correlated for close mass bins.

The results shown in Fig. 5 are very similar to those obtained in S–Au collisions. The invariant mass spectrum of e^+e^- pairs is in good agreement with the predictions from known hadron decays below 200 MeV/c^2 where the expected contribution is dominated by π^0 Dalitz decays. For masses above 200 MeV/c^2 the measured pair yield deviates from the expectations and the yield is clearly enhanced compared to that predicted from hadron decays. This is most pronounced in the region from 300 to 700 MeV/c^2 where the enhancement factor is 5.8 ± 0.8(stat.) $\pm$ 1.5 (syst.). The enhancement extends also to higher masses. In the larger mass interval $0.2 \leq m \leq 2.0$ GeV/c^2 the enhancement factor is 3.5 ± 0.4 (stat) $\pm$ 0.9 (syst).

5.2. Multiplicity dependence

The dependence of the observed dielectron yield on the associated hadron multiplicity is a useful tool to characterize its origin. In spite of the limited statistics of our present Pb–Au sample we tried to exploit the large impact parameter range covered by the data to study the measured yield as a function of the event multiplicity. Fig. 6 shows, on the left

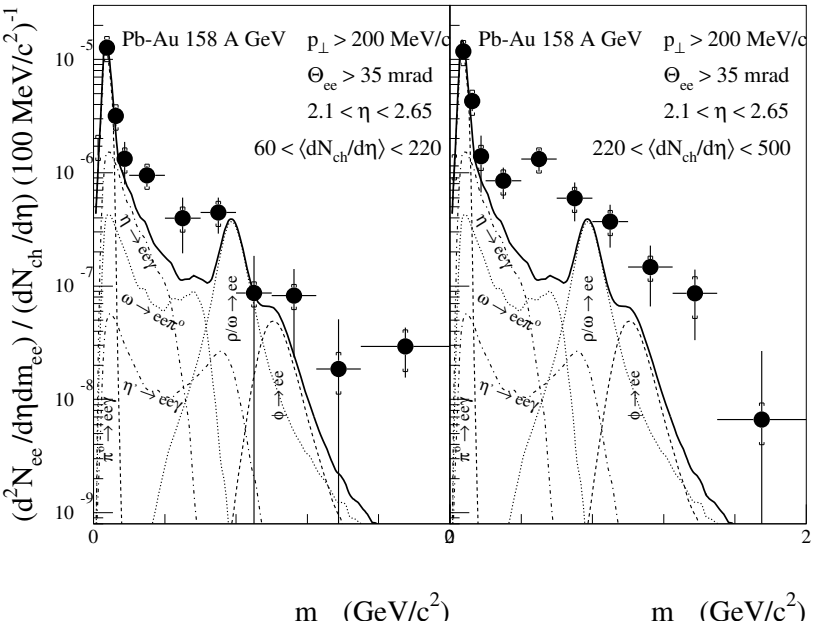

Figure 7. Inclusive e^+e^- mass spectra in 158 A GeV Pb–Au collisions normalized to the observed charged-particle density for $dN_{ch}/d\eta < 220$ (left) and $dN_{ch}/d\eta > 220$ (right) multiplicities. See the caption of Fig. 2 for more details.

panel, the charged-particle multiplicity distribution $dN_{ch}/d\eta$ for $2 < \eta < 3$ as measured in the target telescope and corrected for efficiency and pile-up in the silicon detectors. The distribution is divided into four bins with approximately equal number of events. The right panel of Fig. 6 shows the pair density per charged particle density integrated over the mass range m > 200 MeV/c^2 for each of the four multiplicity bins. Fig. 6 includes also the results from our p–Be and p–Au data samples [3]. If hadron decays were to be the only source of dielectron pairs –as it is the case in pp and pA collisions– the data should scale linearly with multiplicity, i.e. should follow the horizontal line shown in the plot. Although the error bars are large, the data clearly indicate a non-linear dependence as a function of multiplicity. The scale on the right in Fig. 6 (right) represents the enhancement factor for each multiplicity bin reaching a value 5.3 ± 0.8 (stat) ± 1.3 (syst) for central collisions.

The spectral shape of the dilepton excess seems also to change significantly as a function of the charged-particle rapidity density. The effect is illustrated in Fig. 7. Due to the limited statistics the charged particle distribution was divided only into two bins of approximately the same number of events.

5.3. Transverse momentum distributions

We have also extracted the pair transverse-momentum spectra for three invariant-mass regions. The experimental data are plotted in Fig. 8. One should note that the single-track p_t-cut strongly affects the p_t distribution for masses below 400 MeV/c^2, dominating the shape of the pair p_t-spectra at low p_t. The generator curves shown are folded with the momentum resolution and normalized as was discussed above. For masses below 200 MeV/c^2 the p_t distribution agrees with the prediction for π^0 Dalitz decays (left panel). For higher masses, the enhancement is visible over the entire p_t range but it increases significantly towards very low p_t for m$\geq$ 200 MeV/c^2.

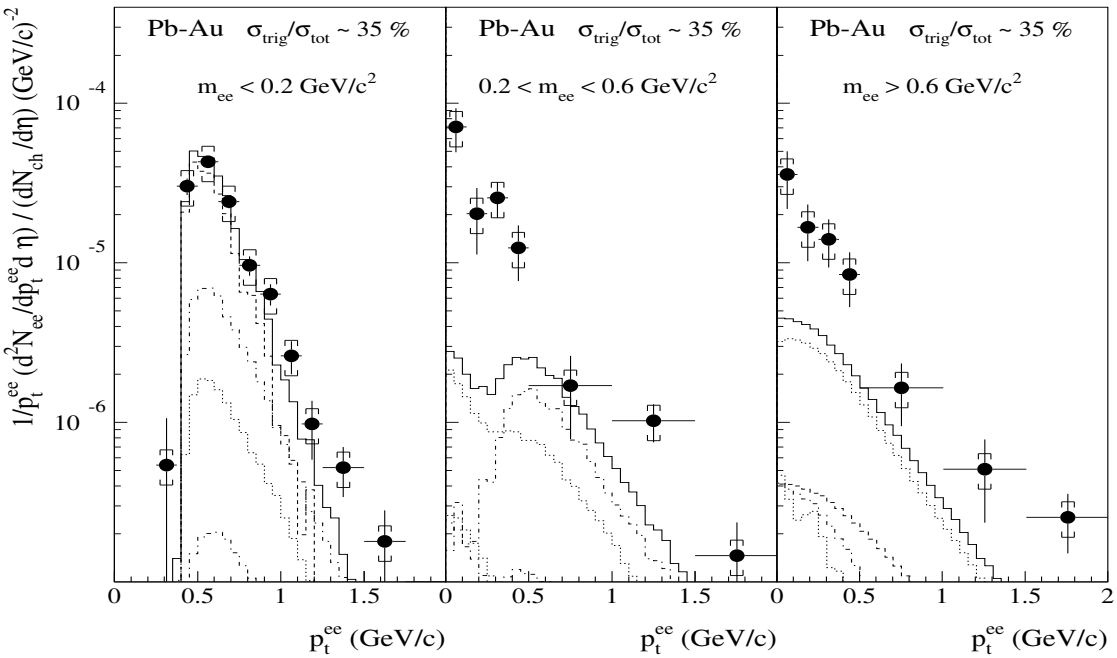

Figure 8. Inclusive e^+e^- pair p_t spectra in 158 GeV/nucleon Pb–Au collisions for three different pair mass ranges. Statistical and systematic errors are given separately. The histograms give the p_t-distributions expected from individual meson decay channels and their sum. The normalization of the hadron decay contribution is identical to the one used in Fig. 5.

6. SUMMARY AND OUTLOOK

We have presented CERES results on low-mass electron pair production in 158 A GeV Pb–Au collisions. The results confirm the significant excess of dielectron pairs observed by CERES, HELIOS-3 and NA38 in S-Au collisions at 200 A GeV. For central Pb–Au and S–Au collisions the shape of the spectrum and the magnitude of the enhancement are similar. We have found evidence for a non-linear dependence on the multiplicity. First data on p_t-spectra show that the yield is enhanced over the entire range, but the increase is strongest at the lowest p_t measured.

Much more precise data on all these findings is expected from the ongoing analysis of the high-statistics run which took place in the fall of 1996. To further elucidate the origin of the excess two major new steps are foreseen on a somewhat longer time scale. First, we are planning to improve the mass resolution to be sensitive to the natural width of the omega, by the addition of a TPC downstream of the present double RICH spectrometer. With this resolution, it will be possible to directly measure the yield of all three vector mesons ρ, ω and ϕ including any possible changes in their properties (mass shift or increased width) thereby providing information on whether or not the scenarios invoking chiral symmetry restoration are at the origin of the low-mass excess. Secondly, CERES is proposing a measurement at the lowest energy attainable at the SPS, of about 40 A GeV, where the effect of baryon density on the vector meson masses is expected to be largest.

ACKNOWLEDGEMENT

The CERES collaboration acknowledges the good performance of the CERN PS and SPS accelerators. We are grateful for support by the German BMBF, the U.S. DoE, the MINERVA Foundation, the German-Israeli Foundation for Scientific Research and Development, and the Israeli Science Foundation.

REFERENCES

1. R. Baur *et al.*, (CERES-Collaboration), Nucl. Inst. Meth. **A343** (1994) 87.
2. G. Agakichiev *et al.* (CERES-Collaboration), Neutral meson production in p–Be and p–Au collisions at 450 GeV beam energy, Z. Phys. C. (in print).
3. G. Agakichiev *et al.* (CERES-Collaboration), Systematic study of low-mass electron pair production in p–Be and p–Au collisions at 450 GeV/c, Z. Phys. C. (in print).
4. G. Agakichiev *et al.* (CERES-Collaboration), Phys. Rev. Lett. **75** (1995) 1272.
5. G. Agakichiev *et al.*, (CERES Collaboration), Low-mass e^+e^- pair production in 158 A GeV Pb–Au collisions at the CERN SPS, its dependence on multiplicity and transverse momentum. Phys. Lett. B. (in print).
6. M. Aguilar-Benitez *et al.*, Z. Phys. C. **50** (1991) 405.
7. M. Masera for the HELIOS-3 Collaboration, Nucl. Phys. **A590** (1995) 127c.
8. A. Falco, NA38 collaboration, in these proceedings.
9. I. Tserruya, Proc. Int. Summer School on the Physics of Quark Gluon Plasma, June 3-6, 1997, Hiroshima, Preprint nucl-ex/9801007.
10. A. Drees, Nucl. Phys. **A630** (1998) 449c.
11. G. Agakichiev *et al.*, (CERES Collaboration), Nucl. Phys. **A610** (1996) 317c.
12. G.Q. Li, C.M. Ko and G.E. Brown, Phys. Rev. Lett. **75** (1995) 4007, Nucl. Phys. **A606** (1996) 568 and G.Q. Li, C.M. Ko, G.E. Brown and H. Sorge, Nucl. Phys. **A611** (1996) 539.
13. W. Cassing, W. Ehehalt, and C.M. Ko, Phys. Lett. **B363** (1995) 35; W. Cassing, W. Ehehalt, and I. Králik, Phys. Lett. **B377** (1996) 5.
14. R. Rapp, G. Chanfray, and J. Wambach, Phys. Rev. Lett. **76** (1996) 368; Nucl. Phys. **A617** 472 (1997).
15. W. Cassing, E.L. Bratkovskaya, R. Rapp and J. Wambach, Preprint nucl-th/9708020.
16. D.K. Srivastava, B. Sinha, and C. Gale, Phys. Rev. **C53** (1996) R567; J. Sollfrank *et al.*, Phys. Rev. **C55** (1997) 392; C.M. Hung and E.V. Shuryak, Phys. Rev. **C56** (1997) 453; V. Koch and C. Song, Phys. Rev. **C54** (1996) 1903; R. Baier, M. Dirks, and K. Redlich, Phys. Rev. **D55** (1996) 4344; J. Murray, W. Bauer, and K. Haglin, hep-ph/9611328, to be published; L. Winckelmann *et al.*, Nucl. Phys. **A610** (1996) 116c.
17. R. Pisarski, Phys. Lett. **B110** (1982) 155.
18. G.E. Brown and M. Rho, Phys. Rev. Lett. **66**, (1991) 2720.
19. T. Hatsuda and S.H. Lee, Phys. Rev. **C46** (1992) R34.
20. J. Wambach, in these proceedings.
21. I. Tserruya, in these proceedings.
22. R. Brun *et al.*, CERN DD/EE/84-1 (1984), unpublished.